Applications of level set methods in computational biophysics

Emmanuel Maitre[1], Thomas Milcent[1], Georges-Henri Cottet[1], Annie Raoult[2], Yves Usson[3]

[1] Laboratoire Jean Kuntzmann, Université de Grenoble and CNRS
[2] Laboratoire MAP5, Université Paris Descartes and CNRS
[3] Laboratoire TIMC, Université de Grenoble and CNRS

Abstract

We describe in this paper two applications of Eulerian level set methods to fluid-structure problems arising in biophysics. The first one is concerned with three-dimensional equilibrium shapes of phospholipidic vesicles. This is a complex problem which can be recast as the minimization of the curvature energy of an immersed elastic membrane, under a constant area constraint. The second deals with isolated cardiomyocyte contraction. This problem corresponds to a generic incompressible fluid-structure coupling between an elastic body and a fluid. By the choice of these two quite different situations, we aim to bring evidences that Eulerian methods provide efficient and flexible computational tools in biophysics applications.

1   Introduction

Biophysics and biomechanics are two fields where Fluid-Structure interactions play an important role, both from the modeling and computing points of view. In many 3D applications, flow and solid models coexist with biochemical systems. For such problems it is desirable to have at hand computing tools wich readily couple models of different nature (typically Eulerian for fluids, Lagrangian for solids), easily enforce continuity conditions at the interface and enable to handle reaction-diffusion systems.

In a series of papers [4, 5, 6] such models where derived to compute the interaction of 3D incompressible fluids with elastic membranes or bodies. These models are based on Eulerian formulations of elasticity and rely on the use of level set functions, both to capture the fluid-solid interfaces and to measure the elastic stresses. Interface conditions are implicitly enforced through the elastic forces acting on the flow equations. They can be seen as alternative to more conventional ALE methods where Eulerian and Lagrangian formulations of the fluid and the solid are coupled through explicit enforcement of interface conditions.

The goal of the present paper is to present applications of this method to two types of problems arising in biophysics. The first problem is the computation of equilibrium shape of biological vesicles. In this case the fluid structure model is a dynamical model for shape optimization, in the spirit of [12], in contrast with more classical geometric approaches [21, 7]. Elastic stresses and immersion of the vesicle in an incompressible fluids are used to enforce constraints of constant area and volume. In the second problem we are concerned with numerical simulations of spontaneous cardiomoyocyte contractions. In that case, the model couples an incompressible anisotropic medium with a reaction-diffusion system for the calcium concentrations. This coupling is through a calcium dependent active stress in the elastic medium. Our approach differs from that in [24, 16] by the fact that no remeshing of the structure is needed during the cell deformation. This leads to substancial computational savings.

An outline of the paper is as follows. In section 2 we focus on the problem of equilibrium shapes for biological vesicles. We present our level set formulation for the shape optimization and show numerical

results for biological vesicles. In section 3 we turn to the elastic deformation of a cardiomyocyte. We recall the level set Eulerian formulation derived in [6] for a transverse isotropic elastic body. We couple this model with the reaction diffusion model [8] and show numerical results illustrating the association of cell contraction with calcium waves. Section 4 is devoted to some concluding remarks.

2 Equilibrium shapes of 3D phospholipidic vesicles

Phospholipidic vesicles are routinely considered as physical models in particular for red blood cells. Their membrane is a bilayer made of a fixed amount of molecules. As a result, it only responds to change of area or breakup. Taking into account the hydrodynamics is necessary in order to be able to study the behavior of these 3D cells when they are immersed in a flowing fluid. Phase-field models have been developed and used in 2D simulations, but 3D simulation of vesicles dynamics in shear flow is still a challenging problem. As a first step in this direction we consider here the problem of finding equilibrium shapes of these vesicles, constrained to have a fixed volume and area. An important parameter is the volume ratio

$$\eta = \frac{3V(4\pi)^{1/2}}{A^{3/2}} \tag{1}$$

where V is the volume and A is the area, which measures the ratio between the volume of the cell and the volume of the sphere having the same area.

Our computational approach mimics the underlying biophysical dynamics, in the sense that we assume that the cell is moving in an incompressible fluid and is subject to a very stiff elastic stress localized on the membrane. The curvature energy that the vesicle is supposed to minimize is used to derive an external force driving it towards its equilibrium.

2.1 Level set formulation

In this section we give a level set formulation for the curvature driven dynamics of elastic membranes immersed in an incompressible fluid. Consider a domain Ω of $\mathbb{R}^3$ containing some incompressible fluid into which a vesicle is immersed. This vesicle is considered to be an elastic surface. One way to describe the motion of this surface is to introduce a function φ whose zero level set is the surface [17]. Given a signed distance function φ^0 such that the initial interface is given by

$$\Gamma_0 = \left\{ x \in \Omega, \quad \varphi^0(x) = 0 \right\},$$

the problem of localizing the structure is reduced to an advection of the function φ by the fluid velocity u. The velocity is solution to a Navier-Stokes system with a singular source term which accounts for the elastic forces acting on the fluid. As observed in [4], when u is incompressible, the change of area of $\{\varphi = 0\}$ is recorded in $|\nabla\varphi|$. Following [5], this makes it possible to express the area energy in terms of φ alone:

$$E_a[\varphi] = \int_\Omega E(|\nabla\varphi|)\frac{1}{\varepsilon}\zeta(\frac{\varphi}{\varepsilon})dx$$

and the associated force is given by

$$f_a[\varphi] = \left\{ \mathbb{P}_{\nabla\varphi^\perp}\left(\nabla[E'(|\nabla\varphi|)]\right) - E'(|\nabla\varphi|)\kappa(\varphi)\frac{\nabla\varphi}{|\nabla\varphi|}\right\}|\nabla\varphi|\frac{1}{\varepsilon}\zeta(\frac{\varphi}{\varepsilon}). \tag{2}$$

In this formula ζ is a cut-off function classically used in level set method to spread the singular force on the mesh. The given function $r \to E'(r)$ describes the response of the membrane to a change of area. As we already pointed out, in the present application the membrane is nearly inextensible, and

choose $E'(r) = \lambda(r-1)$ for large values of λ. This somehow corresponds to penalizing the change of area.

In order to account for curvature effects, we next introduce the following energy:

$$E_c[\varphi] = \int_\Omega G(\kappa(\varphi))|\nabla\varphi|\frac{1}{\varepsilon}\zeta(\frac{\varphi}{\varepsilon})dx$$

where $\kappa(\varphi)$ is the mean curvature. A common choice for $G(r) = \frac{1}{2}r^2$ but terms identification is made easier in the following by keeping a general function G. The strategy to compute the curvature force is to take the time derivative of the energy and identify it with the power of the generated force:

$$\frac{dE_c}{dt} = -\int_\Omega f_c \cdot u dx.$$

Let us first compute the differential of E_c:

$$dE_c[\varphi](\delta) = \int_\Omega G'(\kappa(\varphi)) \operatorname{div}\left(\frac{\nabla\delta}{|\nabla\varphi|} - \frac{\nabla\varphi\cdot\nabla\delta}{|\nabla\varphi|^3}\right)|\nabla\varphi|\frac{1}{\varepsilon}\zeta(\frac{\varphi}{\varepsilon})dx$$
$$+ \int_\Omega G(\kappa(\varphi))\frac{\nabla\varphi\cdot\nabla\delta}{|\nabla\varphi|}\frac{1}{\varepsilon}\zeta(\frac{\varphi}{\varepsilon}) + G(\kappa(\varphi))|\nabla\varphi|\frac{1}{\varepsilon^2}\zeta'(\frac{\varphi}{\varepsilon})\delta dx.$$

The two terms in the second integral may be combined: upon integrating the first one by parts, one obtains

$$-\int_\Omega G(\kappa(\varphi))\kappa(\varphi)\frac{1}{\varepsilon}\zeta(\frac{\varphi}{\varepsilon})\delta + G(\kappa(\varphi))\frac{\nabla\varphi}{|\nabla\varphi|}\frac{1}{\varepsilon^2}\zeta'(\frac{\varphi}{\varepsilon})\nabla\varphi\delta + \nabla G(\kappa(\varphi))\cdot\frac{\nabla\varphi}{|\nabla\varphi|}\frac{1}{\varepsilon}\zeta(\frac{\varphi}{\varepsilon})\delta.$$

Therefore

$$dE_c[\varphi](\delta) = \int_\Omega G'(\kappa(\varphi))\operatorname{div}\left(\frac{\mathbb{P}_{\nabla\varphi^\perp}(\nabla\delta)}{|\nabla\varphi|}\right)|\nabla\varphi|\frac{1}{\varepsilon}\zeta(\frac{\varphi}{\varepsilon}) - G(\kappa(\varphi))\kappa(\varphi)\frac{1}{\varepsilon}\zeta(\frac{\varphi}{\varepsilon})\delta - \nabla G(\kappa(\varphi))\cdot\frac{\nabla\varphi}{|\nabla\varphi|}\frac{1}{\varepsilon}\zeta(\frac{\varphi}{\varepsilon})\delta dx$$

which from the expression of the mean curvature $\kappa(\varphi)$ also reads

$$dE_c[\varphi](\delta) = \int_\Omega G'(\kappa(\varphi))\operatorname{div}\left(\frac{\mathbb{P}_{\nabla\varphi^\perp}(\nabla\delta)}{|\nabla\varphi|}\right)|\nabla\varphi|\frac{1}{\varepsilon}\zeta(\frac{\varphi}{\varepsilon}) - \operatorname{div}(G(\kappa(\varphi))\frac{\nabla\varphi}{|\nabla\varphi|})\frac{1}{\varepsilon}\zeta(\frac{\varphi}{\varepsilon})\delta dx.$$

Since $\mathbb{P}_{\nabla\varphi^\perp}(\nabla\delta)\cdot\nabla\varphi = 0$ the first term may be integrated by parts to give

$$-\int_\Omega \nabla\left[|\nabla\varphi|G'(\kappa(\varphi))\right]\cdot\mathbb{P}_{\nabla\varphi^\perp}(\nabla\delta)\frac{1}{|\nabla\varphi|}\frac{1}{\varepsilon}\zeta(\frac{\varphi}{\varepsilon}) = -\int_\Omega \mathbb{P}_{\nabla\varphi^\perp}\left[|\nabla\varphi|\nabla G'(\kappa(\varphi))\right]\cdot\frac{\nabla\delta}{|\nabla\varphi|}\frac{1}{\varepsilon}\zeta(\frac{\varphi}{\varepsilon})dx$$

where the symmetry of the projector on $\nabla\varphi^\perp$ has been used. Integrating once more by parts we find

$$dE_c[\varphi](\delta) = \int_\Omega \operatorname{div}\left[-G(\kappa(\varphi))\frac{\nabla\varphi}{|\nabla\varphi|} + \frac{1}{|\nabla\varphi|}\mathbb{P}_{\nabla\varphi^\perp}\left(\nabla[|\nabla\varphi|G'(\kappa(\varphi))]\right)\right]\frac{1}{\varepsilon}\zeta(\frac{\varphi}{\varepsilon})\delta dx.$$

Let us now compute the time derivative of the energy. Using the advection equation on φ,

$$\frac{d}{dt}E_c[\varphi] = dE_c[\varphi](\varphi_t) = dE_c[\varphi](-u\cdot\nabla\varphi) = -\int_\Omega f_c(x,t)\cdot u dx \tag{3}$$

which by identification gives:

$$f_c[\varphi] = \operatorname{div}\left[-G(\kappa(\varphi))\frac{\nabla\varphi}{|\nabla\varphi|} + \frac{1}{|\nabla\varphi|}\mathbb{P}_{\nabla\varphi^\perp}\left(\nabla[|\nabla\varphi|G'(\kappa(\varphi))]\right)\right]\frac{1}{\varepsilon}\zeta(\frac{\varphi}{\varepsilon})\nabla\varphi. \tag{4}$$

3

A more general derivation of curvature driven level set models for shape optimization will be given in [11].

The two forces (2) and (4) are finally inserted as forcing terms in the Navier-Stokes equations, leading to the following model: given and initial velocity field u_0 and an initial interface φ_0, find (u, φ) solution to

$$
\begin{cases}
\rho(\varphi)(u_t + u \cdot \nabla u) - \operatorname{div}(\mu(\varphi)D(u)) + \nabla p = f_a[\varphi] + f_c[\varphi] & \text{on } \Omega \times]0, T[\\
\operatorname{div} u = 0 & \text{on } \Omega \times]0, T[\\
\varphi_t + u \cdot \nabla \varphi = 0 & \text{on } \Omega \times]0, T[\\
u = u_0 \quad \varphi = \varphi_0 & \text{on } \Omega \times \{0\}
\end{cases}
$$

where ρ and μ are the, possibly varying, density and viscosity of the complex fluid. The boundary condition to be enforced at the boudary of the computational box Ω plays a marginal role. For simplicity we in general choose homogeneous Dirichlet boundary condtions.

Note that for this model the following energy equality holds for all $t \in [0, T]$:

$$
\frac{1}{2} \int_\Omega \rho(\varphi)u^2 \, dx + \int_\Omega E(|\nabla \varphi|) \frac{1}{\varepsilon} \zeta(\frac{\varphi}{\varepsilon}) \, dx + \int_\Omega G(\kappa(\varphi))|\nabla \varphi| \frac{1}{\varepsilon} \zeta(\frac{\varphi}{\varepsilon}) dx + \frac{1}{2} \int_0^t \int_\Omega \mu(\varphi)D(u)^2 \, dx \, dt
$$

$$
= \frac{1}{2} \int_\Omega \rho(\varphi_0)u_0^2 \, dx + \int_\Omega E(|\nabla \varphi_0|) \frac{1}{\varepsilon} \zeta(\frac{\varphi_0}{\varepsilon}) \, dx + \int_\Omega G(\kappa(\varphi_0))|\nabla \varphi_0| \frac{1}{\varepsilon} \zeta(\frac{\varphi_0}{\varepsilon}) dx
$$

which shows that the spreading of elastic and curvature forces inherent to the level set method does not introduce any energy dissipation. We also remark that the resolution of the full problem fluid/membrane, while not mandatory to obtain equilibrium shapes (but mandatory to study the dynamical behavior of vesicles in shear flow), brings some advantages from the viewpoint of volume conservation: indeed we will use a projection method which will ensure this conservation at the discrete level. Note that in order to solve the minimization problem without any fluid, it is necessary to add a volume constraint which is usually enforced through a Lagrange multiplier approach. This may result in a loss of accuracy for volume conservation.

2.2 Numerical results

The numerical results presented here show two typical situations of optimal shapes for 3D vesicles. The final shape depends on the volume ratio coefficient η defined in (1). The first test case corresponds to $\eta = 0.8$, giving a peanut minimizing shape (figure 1, top pictures). The second one to $\eta = 0.586$ looks like a real red blood cell (figure 1, bottom pictures). In each series of pictures we have represented a sequence of shapes from the initialization stage (left pictures) to the steady-state optimal shapes (right pictures). These shapes qualitatively agree with those observed for corresponding η values ([19]). Ongoing works deal with the extension of the present method to simulate the dynamical behavior of 3D vesicles in shear flows.

The numerical resolution of Navier-Stokes equations is performed using a finite differences solver (projection method) on a MAC mesh [1] of size 128^3. In order to ensure volume conservation which is crucial in this problem, the level set function is advected using a fifth order WENO scheme. Since the level set function is used through its gradient to compute the stretching, we do not perform the usual redistancing operation on the level set function [17]. Instead, we use the renormalization $\frac{\varphi}{|\nabla \varphi|}$ to measure the distance to interface. This approach was proved in [5] to be efficient from the point of view of both volume conservation and interface force calculations.
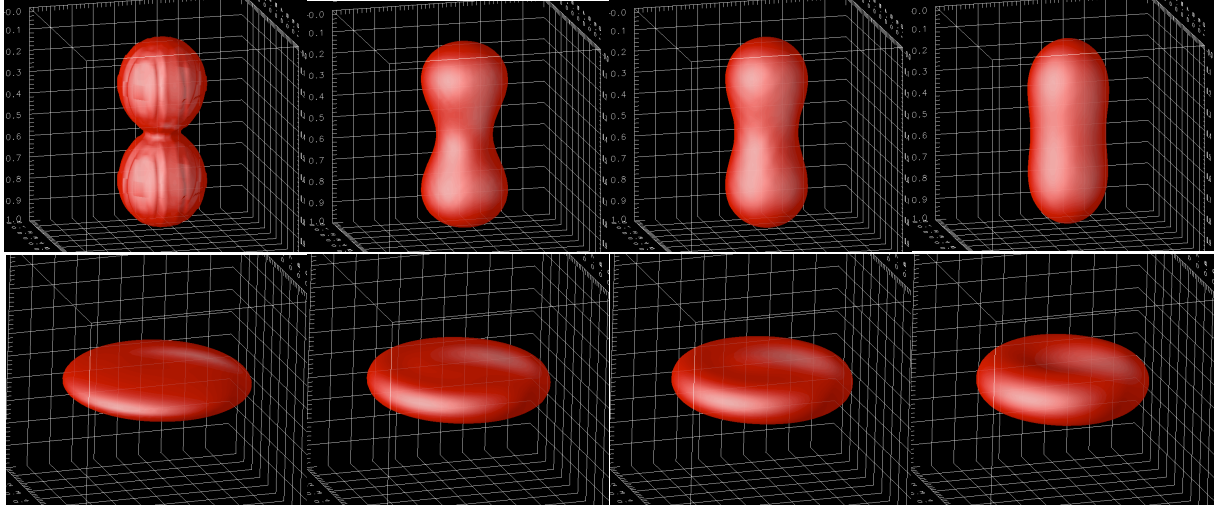
FIGURE 1: Shape optimization for equilibrium shapes of biological shapes. Top pictures: $\eta = 0.8$, bottom pictures: $\eta = 0.586$. Initialization to steady-state from left to right.

3 Eulerian three-dimensional modelisation and simulation of cardiomyocytes contraction induced by calcium waves

In a recent article, Okada and al [16] investigated the mechanism of calcium wave propagation in connection with cardiomyocyte contraction. They developed a $3D$ simulator using the model of [22] for the Ca^{2+} dynamics and relying on the Negroni and Lascano's contraction model [14] which couples Ca^{2+} concentration with force generation. For the elastic part an isotropic Saint-Venant hyperelastic model was assumed and myofibrills, Z-lines sarcolemma, cytoskeleton and cytoplasm were represented by various finite elements famillies. In our paper we adopt a similar approach in an Eulerian framework: following [6] we use a level set approach of the fluid-structure coupling the surrounding fluid and the cardiomyocyte, considering these two as an unique incompressible continuous medium. The microscopic internal structure of the cardiomyocyte is not described: the passive property of the myocyte is given by nonlinear elasticity, with a transverse isotropy assumption accounting for the topology of sarcolemma. The calcium dynamics is coupled through an active stress law given by Stuyvers and al. [23], as described in Tracqui and al. [24]. While our model does not pretend to reproduce the internal structure as precisely as in [16] , it is more realistic in some respects in the elastic part. In particular it is worth noticing that the Saint-Venant constitutive law considered in [16] should not be used for the large deformations observed in myocytes.

3.1 Description of the model

In this section we rely on the level set framework developed in [6] for anisotropic elastic bodies in interaction with incompressible fluids and couple this model with a differential system for the Calcium concentration responsible for the active stress.

3.1.1 Eulerian formulation of the passive continuous medium

The cardiomyocyte is immersed in a fluid which lies in a bounded domain $\Omega \subset \mathbb{R}^3$. We denote by u the divergence-free velocity field of the whole continuous medium, assumed to be $\mathcal{C}^1$ and to vanish on

the boundary $\partial\Omega$.

$$(H) \qquad u \in \mathcal{C}^1(\overline{\Omega} \times [0,T]) \text{ and } u = 0 \text{ on } \partial\Omega \times [0,T]$$

The interface between the cardiomyocyte and the fluid is captured by a level set function ψ_0. Note that ψ_0 needs not be a sign function. In our calculations it was obtained from experimental data, specifically by confocal miscroscopy [25]. Let us introduce the characteristics of the vector field u. We denote by $s \to X(s; x, t) \in \mathbb{R}^3$ the solution of the differential system

$$\frac{\partial X}{\partial s} = u(X, s)$$

with "initial" condition $X(t; x, t) = x$. Classically, under the assumptions (H), the map $x \to X(s; x, t)$ is a $\mathcal{C}^1$ diffeomorphism from Ω to Ω. Since u is incompressible, one has div $u = 0$ and thus the Jacobian of X, denoted by J, is equal to 1. Following [6], to compute X in an Eulerian fashion, we use the following transport equation satisfied by X as a funtion of t, x :

$$X_t(s; x, t) + u(x, t) \cdot \nabla X(s; x, t) = 0 \tag{5}$$

still with the same initial condition on $t = s$. Once X is computed at time t (for $s = 0$), several quantities can be easily obtained. The cardiomyocyte boundary position is given by the zero level set of $\psi(x, t) = \psi_0(X(0; x, t))$. The left Cauchy-Green tensor is given by ([2], p. 15, [3], p. 43)

$$B = FF^t \text{ where } F(x, t) = (\nabla X)(t; X(0; x, t), 0) = (\nabla X)^{-1}(0; x, t)$$

the last equality being obtained by differentiation of $X(t; X(0, x, t), 0) = x$. For an elastic material whose response is frame-independent and isotropic at point $\xi = X(0; x, t)$, the Cauchy stress tensor at x is given by ([2], p. 50, [3], p. 115)

$$T(x) = T^D(x, B(x, t)).$$

If this material is incompressible, then this constitutive equation becomes ([10], p. 45, or [3], p. 259 after applying a Piola transform):

$$\sigma^S(x) = T^D(x, B(x, t)) - p(x)\mathbb{I}$$

where $\mathbb{I}$ is the identity. If we describe the surrounding fluid as Newtonnian, the stress tensor in this part of the continuous medium is given by

$$\sigma^F(x) = -p(x)\mathbb{I} + \mu D(u)$$

where μ stands for the viscosity and $D(u) = \frac{1}{2}(\nabla u + \nabla u^t)$. The conservation of momentum may thus be written as

$$\rho(u_t + u \cdot \nabla u) - \text{div } \sigma + \nabla p = f$$

where $\sigma = \sigma^S \chi_{\{\psi<0\}} + \sigma^F \chi_{\{\psi>0\}}$ and $\sigma^S = T^D(x, B(x, t))$, $\sigma^F = \mu D(u)$. Of course the momentum equation has to be understood in the sense of distributions. For computational purposes, a regularization of χ using the level set function ψ must be introduced. If we denote by $r \to H(\frac{r}{\varepsilon})$ an approximation of the Heaviside function, the regularized stress

$$\sigma_\varepsilon = \sigma^S(1 - H(\frac{\psi}{\varepsilon})) + \sigma^F H(\frac{\psi}{\varepsilon})$$

varies smoothly across the interface $\psi = 0$ and the momentum equation may be understood in the classical sense.

3.1.2 Transverse isotropy

In the myocardic tissue, cells are assembled along fibres and bundled by collagen, and in each myocyte the sarcolemma are parallel to this direction. Thus anisotropy is expected. More precisely, following [13], p. 80, the myocardic tissue can be considered as transverse isotropic [15]. Let τ be the preferred direction for the cardiomyocyte, i.e. its long axis at rest. Such a material can be characterized with a strain energy which depends on F and $\tau \otimes \tau$. The stress tensor has then the following general expression

$$\sigma^S = -p\mathbb{I} + 2\alpha_1 B + 2\alpha_2(\operatorname{tr}(B)B - B^2) + 2\alpha_4 F\tau \otimes F\tau + 2\alpha_5(F\tau \otimes BF\tau + BF\tau \otimes F\tau) \quad (6)$$

where α_i is the derivative of the strain energy with respect to the invariant number i, with

$$I_1 = \operatorname{tr}(B), \quad I_2 = \frac{1}{2}[\operatorname{tr}(B)^2 - \operatorname{tr}(B^2)], \quad I_4 = |F\tau|^2, \quad I_5 = (BF\tau) \cdot (F\tau). \quad (7)$$

While $I_4^{\frac{1}{2}}$ stands for the fibre elongation (prefered direction), $I_5^{\frac{1}{2}}$ measure the elongation in the direction normal to the unprefered directions. For the sake of simplicity we will restrict ourselves in this paper to the case where $\alpha_5 = 0$. As the quantity computed by resolution of (5) is $(x,t) \to X(0;x,t)$, we have to express the stress law in terms of its components $X_i(0;x,t)$, $i = 1,2,3$. As $F = (\nabla X)^{-1}(0;x,t)$, and $\det F = 1$ by incompressibility, this is easily done:

$$F(x,t) = \operatorname{cof} \nabla X^t = \begin{pmatrix} X_{,x_2} \times X_{,x_3} \\ X_{,x_3} \times X_{,x_1} \\ X_{,x_1} \times X_{,x_2} \end{pmatrix} = \begin{pmatrix} \nabla X_2 \times \nabla X_3 & \nabla X_3 \times \nabla X_1 & \nabla X_1 \times \nabla X_2 \end{pmatrix}$$

where $X_{,x_i} \times X_{,x_j}$ are row vectors, and $\nabla X_i \times \nabla X_j$ column vectors. The components of $B = FF^t$ are thus obtained from two-by-two scalar products of the $X_{,x_i} \times X_{,x_j}$. For the invariants I_1 and I_2 involved in (7), after some elementary computations, there holds

$$I_1 = \operatorname{tr}(B) = |X_{,x_2} \times X_{,x_3}|^2 + |X_{,x_3} \times X_{,x_1}|^2 + |X_{,x_1} \times X_{,x_2}|^2 = |\operatorname{cof} \nabla X|^2$$

$$\operatorname{tr}(B^2) = \operatorname{tr}(B)^2 - 2(|X_{,x_1}|^2 + |X_{,x_2}|^2 + |X_{,x_3}|^2), \quad I_2 = |X_{,x_1}|^2 + |X_{,x_2}|^2 + |X_{,x_3}|^2 = |\nabla X|^2 \quad (8)$$

After some tedious yet elementary algebra, using $(X_{,x_1} \times X_{,x_2}) \cdot X_{,x_3} = 1$, $(\operatorname{tr} B)B - B^2$ has the following simple expression:

$$(\operatorname{tr} B)B - B^2 = \begin{pmatrix} |X_{,x_2}|^2 + |X_{,x_3}|^2 & -X_{,x_1} \cdot X_{,x_2} & -X_{,x_1} \cdot X_{,x_3} \\ -X_{,x_1} \cdot X_{,x_2} & |X_{,x_1}|^2 + |X_{,x_3}|^2 & -X_{,x_2} \cdot X_{,x_3} \\ -X_{,x_1} \cdot X_{,x_3} & -X_{,x_2} \cdot X_{,x_3} & |X_{,x_1}|^2 + |X_{,x_2}|^2 \end{pmatrix}$$

and $\alpha_1, \alpha_2, \alpha_4$ are functions of $|\operatorname{cof} \nabla X|^2, |\nabla X|^2, |\operatorname{cof} \nabla X^t \tau|^2$.

3.1.3 Active contraction and final model

We now come to the coupling of the elastic properties with the biochemistry taking place inside the cell. For the active behavior of the cardiomyocyte, we follow [24] where the active stress is added to σ^S. With our notations it corresponds to adding in (6) the term

$$T_0\gamma(Z(x,t))$$

to α_4, where Z is the intracellular Ca^{2+} concentration, and γ is the following Hill function [23]:

$$\gamma(Z) = \frac{Z^{n_H}}{Z_{50}^{n_H} + Z^{n_H}}$$

The constant T_0 was fixed to $5.5kPa$ such that predicted and experimental amplitudes match. The calcium dynamics is given by the following reaction-diffusion system [22, 8]:

$$\frac{\partial Y}{\partial t} = \nu_2(Z) - \nu_3(Y, Z) - k_f Y \tag{9}$$

$$\frac{\partial Z}{\partial t} = \nu_0 + \nu_1\beta - \nu_2(Z) + \nu_3(Y, Z) + k_f Y - kZ + \nabla \cdot (\mathbf{D}\nabla Z) \tag{10}$$

$$Z(r, t_0) = Z_0; \; Y(r, t_0) = Y_0 \tag{11}$$

where the diffusion tensor is diagonal. As experimentally observed by [22], we considered a ratio $\frac{D_{33}}{D_{11}} = \frac{D_{22}}{D_{11}} = 0.5$ between diffusion along the sarcolemma direction and the transverse directions. The calcium fluxes ν_2 and ν_3 are given by the following Michaelis-Menten functions:

$$\nu_2 = V_{M_2}\frac{Z^n}{K_2^n + Z^n} \tag{12}$$

$$\nu_3 = V_{M_3}\frac{Y^m}{K_R^m + Y^m}\frac{Z^p}{K_A^p + Z^p} \tag{13}$$

We refer to [24] for precise biological meaning of constants and function appearing in (9)-(13), and to table 2 for the values used in the forthcoming numerical simulations.

The final model consists of the following set of equations:

$$\rho(u_t + u \cdot \nabla u) - \text{div}\,\sigma_\varepsilon + \nabla p = f$$

$$\sigma_\varepsilon = \sigma^S(1 - H(\frac{\psi}{\varepsilon})) + \sigma^F H(\frac{\psi}{\varepsilon})$$

with $\sigma^S = -p\mathbb{I} + 2\alpha_1 B + 2\alpha_2(\text{tr}(B)B - B^2) + 2(\alpha_4 + T_0\gamma(Z(x, t)))F\tau \otimes F\tau$ and $\sigma^F = \mu D(u)$, coupled with the system (9-11).

Parameter	Value	Unit
ν_0	0.45	$\mu M.s^{-1}$
k	2.2	s^{-1}
ν_1	4	$\mu M.s^{-1}$
V_{M_2}	65	$\mu M.s^{-1}$
V_{M_3}	500	$\mu M.s^{-1}$
K_2	1.2	μM
K_A	0.92	μM
K_R	3.5	μM
Y_0	0.1	μM
Z_0	10	μM
Z_{50}	2.5	μM
β	0.05	$-$
D_{11}	300	$\mu m^2 s^{-1}$
D_{22}	150	$\mu m^2 s^{-1}$
D_{33}	150	$\mu m^2 s^{-1}$
T_0	5.5	kPa

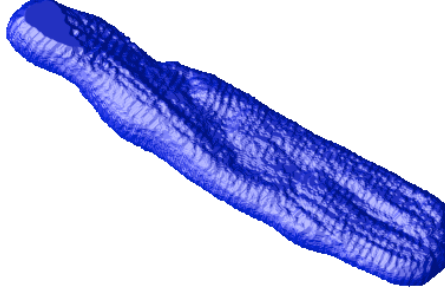Table 2: Parameters values used in numerical simulations

FIGURE 2: Geometry of a cardiomyocyte obtained by confocal imagery [25] as used to initialize the level set function ψ

3.2 Numerical results

For the Navier-Stokes and advection equations we used the finite-difference method described in section 2.2. The reaction-diffusion system was solved on the same mesh using a three-points discretisation of the (diagonal) diffusive terms. We considered two cases. In the first case the calcium concentration is homogeneous in the cell. In the second case the calcium concentration si initialized randomly and produces after some transient a coherent wave propagating across the cardiomyocyte. In both case the cardiomyocyte geometry was acquired from data obtained in [25] using confocal microscopy (see figure 2).

In all our calculation we used a grid of 128^3 points in a box surrounding the cell (the cell itself represented about 50% of the computational box). However, to obtain a better quality visualisation we ran a better resolved transport equation for the level set using velocity values interpolated form the low resolution results. Calcium concentration where represented on the fine mesh by interpolation form the lower resolution calculations.

3.2.1 Uniform contraction

In this first test case (figure 3), the coefficient β which controls the source of calcium is set constant in space. This results in an homogeneous calcium release and in a uniform contraction along the whole body of the cardiomyocyte. Note that this leads to a nonlinear elasticity problem with large displacemements. The cardiomyocyte is discretized on a 384^3 grid for the advection equation, while the fluid-structure equations are solved on a 128^3 grid.

3.2.2 Coupling with a calcium wave

In this case, the coefficient β is a spatially localized function. This triggers a calcium wave which is starting on the left front of the cell and is propagating towards the other end (see figure 4). Note that the propagation is faster along the fiber direction, due to the higher diffusion coefficient in the
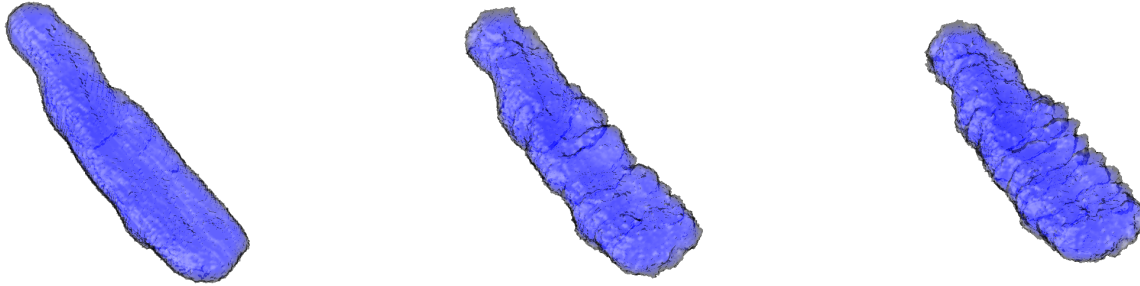
9

FIGURE 3: Uniform contraction of a cardiomyocyte resulting form an homogeneous calcium release

reaction-diffusion CICR system (see table). In that case the calcium peaks come with a deformation in a plane transverse to the principal axis of the cell. The efficiency, in terms of contraction along the principal axis, is clearly much lower than in the previous case. Note that for clarity, in this experiment as in the previous one, the fluid is not represented.

4   Conclusion

We have presented level set methods based on Eulerian representation of elasticity to deal with fluid-structure interactions. Two biophysical examples were provided to illustrate our method in this field, for vesicles shape optimization and cardiomyocyte contraction. These examples focus on interaction of a fluid with an immersed membrane, or an anisotropic elastic material. Both involve elasticity with large displacements, which would be very time consuming to deal with in the classical ALE method.

Acknowledgments

References

[1] D. Brown, R. Cortez and L. Minion, *Accurate Projection Methods for the Incompressible Navier-Stokes Equations*, J. Comp. Phys., 168, 464–499 (2001)

[2] P.G. Ciarlet *Elasticité tridimensionnelle*, Masson (1985)

[3] P.G. Ciarlet *Mathematical elasticity, Volume 1: Three-dimensional elasticity*, North-Holland Publ. (1988)

[4] G.-H. Cottet and E. Maitre, *A level set formulation of immersed boundary methods for fluid-structure interaction problems*, C. R. Acad. Sci. Paris, Ser. I 338, 581–586 (2004)
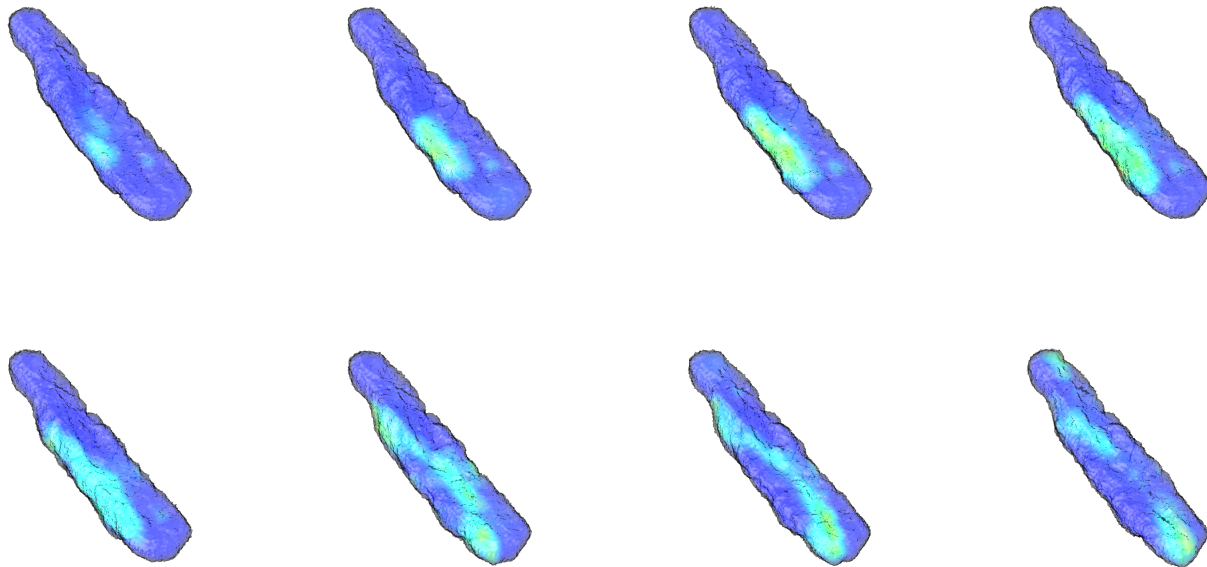
FIGURE 4: Calcium wave propagating into a cardiomyocyte. The color codes for the calcium concentration. Total simulation time: 1s

[5] G.-H. Cottet and E. Maitre, *A level set method for fluid-structure interactions with immersed surfaces*, M3AS, 16 (3), 415–438 (2006)

[6] G.-H. Cottet, E. Maitre, T. Milcent, *Eulerian formulation and level set models for incompressible fluid-structure interaction*, submitted.

[7] Q. Du, C. Liu, R. Ryham and X. Wang, *A phase field formulation of the Willmore problem*, Nonlinearity 18, 1249-1267 (2005)

[8] A. Goldbeter, G. Dupont, M.J. Berridge, *Minimal model for signal-induced Ca^{2+} oscillations and for their frequency encoding through protein phosphorylation*, Proc .Natl. Acad. Sci. USA, 87, 1461–1465 (1990)

[9] M.E. Gurtin, *An introduction to continuum mechanics*, Mathematics in Science and Engineering Series, Vol. 158, Academic Press (1981)

[10] M.E. Gurtin, *Topics in finite elasticity*, CMBS-NSF Regional Conference Series in Applied Mathematics, SIAM, Philadelphia (1981)

[11] E. Maitre and T. Milcent, *A comparison between level set and classical shape optimization for curvature dependent functionals*, in preparation.

[12] T. Biben, C. Misbah, A. Leyrat and C. Verdier, *An advected field approach to the dynamics of fluid interfaces'*, Euro. Phys. Lett. 63, 623 (2003)

[13] A. Mourad, *Description topologique de l'architecture fibreuse et modlisation mcanique du myocarde*, PhD Thesis INPG, Grenoble (2003)

[14] J.A. Negroni and E.C. Lascano, *A cardiac muscle model relating sarcomere dynamics to calcium kinetics*, J. Mol. Cell. Cardiol. 28: 915–929 (1996)

[15] R.W. Ogden, *Nonlinear elasticity, anisoptropy, material staility and residual stresses in soft tissue*, Biomechanics of Soft Tissue in Cardiovascular Systems (edited by G.A. Holzapfel and R.W. Ogden), CISM Course and Lectures Series 441, Springer, Wien, 65–108 (2003)

[16] J. Okada, S. Sugiura, S. Nishimura, and T. Hisada, *Three-dimensional simulation of calcium waves and contraction in cardiomyocytes using the finite element method*, Am. J. Physiol. Cell. Physiol. 288: C510–C522 (2005)

[17] S. Osher and R. P. Fedkiw, *Level set methods and Dynamic Implicit Surfaces*, Springer (2003)

[18] C.S. Peskin, *The immersed boundary method*, *Acta Numerica*, **11**, 479–517 (2002)

[19] U. Seifert, K. Berndl, and R. Lipowsky, *Shape transformations of vesicles: phase diagram for spontaneous curvature and bilayer coupling model*, Phys. Rev. A., 44:1182 (1991)

[20] C.-W. Shu, *Essentially non-oscillatory and weighted essentially non-oscillatory schemes for hyperbolic conservation laws*, ICASE Report No. 97-65
`http://techreports.larc.nasa.gov/icase/1997/icase-1997-65.pdf`

[21] L. Simon, *Existence of surfaces minimizing the Willmore functional*, Comm. Anal. Geom. 1, 281–326 (1993)

[22] S. Subramanian, S. Viatchenko-Karpinski, V. Lukyanenko, S. Gyrke and T.F. Wiesner, *Underlying mechanisms of symetric calcium wave propagation in rat ventricular myocytes*, Biophys. J. 80: 1–11 (2001)

[23] B.D. Stuyvers, A.D. McCulloch, J. Guo, H.J. Duff, and H.E.D.J. Keurs, *Effect of stimulation rate, sarcomere length and Ca^{2+} on force generation by mouse cardiac muscle*, J. Physiol. 544.3, 817–830 (2002)

[24] A. Pustoc'h, T. Boudou, J. Ohayon, Y. Usson and P. tracqui, *Finite element modelling of the calcium-induced contraction cardiomyocytes based on time-lapse videomicroscopy*, in WSEAS Transactions Information Science and Applications, ISBN 1790-0832, 376–278, (2004)

[25] Y. Usson, F. Parazza, P.-S. Jouk and G. Michalowicz, *Method for the study of the three-dimensional orientation of the nuclei of myocardial cells in fetal human heart by means of confocal scanning laser microscopy*, Journal of Microscopy, 174, 101-110 (1994)